

On the boundary-layer structure of patterns of convection in rectangular-planform containers

By P. G. DANIELS AND A. T. LEE†

Department of Mathematics, City University, Northampton Square, London EC1V 0HB, UK

(Received 19 June 1998 and in revised form 30 April 1999)

This paper considers the structure of steady-state solutions of the Swift–Hohenberg equation describing convection in shallow rectangular-planform containers heated from below. The lateral dimensions of the planform are assumed to be much larger than the characteristic wavelength of convection. Results are restricted to patterns composed of rolls orthogonal to the sides of the rectangle in which case convection sets in at a critical value of the Rayleigh number in the form of rolls parallel to the shorter sides. This primary bifurcation from the conductive state of no motion produces a solution which subsequently undergoes a secondary bifurcation in which the low-amplitude motion near the shorter sides is replaced locally by cross-rolls perpendicular to the sides. This results in the formation of grain boundaries (or domain boundaries) within the fluid which mark the division between the different roll orientations.

With increasing Rayleigh number the grain boundaries approach the sides of the rectangle and a boundary-layer structure is formed. In the present paper the method of matched asymptotic expansions is used to determine this boundary-layer structure and to predict the location of the grain boundaries. An interesting feature of the solution is that the grain boundaries develop significant curvature and bend into the corners of the rectangle, where the local solution is also determined.

The results are compared with numerical computations of the secondary solution branch and with previous numerical and experimental work.

1. Introduction

The task of classifying convective states in shallow rectangular-planform containers heated from below still presents a formidable challenge, both experimentally and theoretically (see, for example, Cross & Newell 1984; Newell, Passot & Souli 1990). A key feature is the formation of stationary states containing grain boundaries. These are boundaries at which roll patterns with different orientations meet in an abrupt fashion, the term being taken from the junction between monocrystals in crystal physics (Friedel 1964). The location and dynamics of such boundaries, as dictated by the geometry of the container, are of some interest. Properties of grain boundaries in the context of thermal convection have been discussed by Manneville & Pomeau (1983), Tesauro & Cross (1987) and Malomed, Nepomnyashchy & Tribelsky (1990), with particular reference to their effect on wavelength selection. The dynamics of curved grain boundaries in convection patterns have been discussed by Hari &

† Present address: Department of Physics, Bucknell University, Lewisburg, PA 17837, USA.

Nepomnyashchy (1994) using an approach developed by Rubinstein, Sternberg & Keller (1989) for studying curved fronts which arise in certain reaction-diffusion problems. Hoyle (1995) has studied stationary grain boundaries in the context of ramped convection, where the boundary is generated by a spatial variation of the Rayleigh number, and applications to travelling waves and in fibre optics have been discussed by Malomed (1994*a*), van Hecke & Malomed (1997) and Malomed (1994*b*).

One reason that grain boundary structures arise in convection in large-planform rectangular containers is that the primary roll pattern becomes susceptible to a cross-roll instability. This instability, first discussed by Schluter, Lortz & Busse (1965) and observed experimentally by Chen & Whitehead (1968) and Croquette (1989*a*), arises in regions where the amplitude of the primary roll pattern is sufficiently low. In the rectangular geometry this typically occurs near each of the shorter lateral sides and results in the formation of cross-rolls there. This has been discussed theoretically by Pomeau & Zaleski (1981) and observed in experiments by Croquette & Schosseler (1982) and Pocheau & Croquette (1984), and in numerical simulations by Arter & Newell (1988). An analysis of the local steady-state structure in the case of a primary roll pattern parallel to an infinitely long, isolated wall was undertaken by Daniels & Weinstein (1992). They demonstrated the existence of a transition line (the grain boundary) parallel to the wall which separates the main roll pattern from a region near the wall containing a bimodal combination of rolls parallel and perpendicular to the boundary. Their analysis incorporated the effect of forcing at the boundary (equivalent to an imperfectly insulated or conducting boundary) and showed that as the imperfection tends to zero the grain boundary moves away from the wall.

For a large rectangular planform with boundary conditions equivalent to perfectly insulating or conducting walls the cross-roll instability results in a secondary bifurcation at which the grain boundaries appear near the shorter sides. Daniels & Weinstein (1996) studied the structure of this secondary bifurcation, for the case where the pattern is restricted to rolls orthogonal to each side of the rectangle, by solving a coupled pair of amplitude equations. These were derived from the Swift–Hohenberg (1977) equation, for which extensive numerical simulations have been carried out (Greenside & Coughran 1984) but are also relevant to the full Rayleigh–Bénard system with rigid upper and lower surfaces at a particular value of the Prandtl number (Sivapragasam 1995). Numerical computations of the steady-state secondary solution branch beyond the bifurcation point showed that having initially moved inwards the grain boundaries then start to approach the walls again as the Rayleigh number increases. In the present paper the computations are extended to much higher Rayleigh numbers within the weakly nonlinear regime. The main purpose of the paper is to determine the asymptotic structure of the solution which emerges with increasing Rayleigh number, or more specifically the solution for Rayleigh numbers much greater than L^{-2} in excess of the critical Rayleigh number for the corresponding infinite layer, where $L \gg 1$ is a typical measure of the ratio of the horizontal dimensions of the container to its depth.

The governing equations and boundary conditions are formulated in §2. Numerical solutions of the amplitude equations obtained using an explicit finite difference scheme are reported in §3. The remainder of the paper is concerned with the asymptotic structure of the solution that emerges with increasing Rayleigh number. This is found to consist of several distinct regions near each shorter side of the rectangle but the key element is a curvature of the grain boundary needed to counterbalance the influence of the wall. This is accommodated by a transformation to coordinates which follow the initially unknown shape of the grain boundary. The main variation in the solution

occurs within a boundary-layer region which encompasses the grain boundary and is considered in §4. The boundary layer itself divides into an outer region which contains only rolls parallel to the wall and an inner region which contains a combination of rolls parallel and perpendicular to the wall. These two regions are separated by a thin transition region which is considered in §5 and can be interpreted as the grain boundary in the sense that it marks the outermost extent of the perpendicular roll component. The shape of the grain boundary is then determined in §6 by matching the solution with that in another layer, immediately adjacent to the wall. An important element of the solution is a requirement that the grain boundary approaches the corners of the rectangle. The solution in the corner regions is considered in §7 and the effect on the core solution is analysed in §8. The results are discussed in §9.

2. Formulation

The Swift–Hohenberg equation is considered in the form

$$\frac{\partial \psi}{\partial t} = \epsilon \psi - (\nabla^2 + 1)^2 \psi - \psi^3, \quad (2.1)$$

where $\psi = \psi(x, y, t)$, $\nabla^2 = \partial^2/\partial x^2 + \partial^2/\partial y^2$ and ϵ is a measure of the amount by which the Rayleigh number exceeds its critical value for an infinite layer. In the weakly nonlinear limit this simplified two-dimensional model contains the essential ingredients of the full Rayleigh–Bénard system and for a rectangular domain $0 \leq x \leq L, 0 \leq y \leq M$ boundary conditions equivalent to rigid, perfectly insulating or conducting sidewalls are

$$\psi = \frac{\partial \psi}{\partial x} = 0 \quad \text{on} \quad x = 0, L, \quad (2.2)$$

$$\psi = \frac{\partial \psi}{\partial y} = 0 \quad \text{on} \quad y = 0, M. \quad (2.3)$$

Steady spatially periodic solutions of (2.1) exist for $\epsilon > 0$, and for small ϵ and large L and M amplitude equations describing orthogonal rolls aligned with the sidewalls are obtained by setting

$$\psi = \frac{2}{\sqrt{3}} L^{-1} \{A(X, Y, \tau) e^{ix} + B(X, Y, \tau) e^{iy}\} + \text{c.c.} + \dots \quad (2.4)$$

Here c.c. denotes complex conjugate, A and B are complex functions representing the amplitudes of rolls with axes perpendicular to the x - and y -directions respectively (x -rolls and y -rolls) and X, Y and τ are defined by

$$x = LX, \quad y = LY, \quad t = \frac{1}{4} L^2 \tau. \quad (2.5)$$

It then follows from (2.1) that for finite values of

$$\delta = \frac{1}{4} \epsilon L^2, \quad (2.6)$$

A and B satisfy the coupled pair of amplitude equations

$$\frac{\partial A}{\partial \tau} = \frac{\partial^2 A}{\partial X^2} + \delta A - A(|A|^2 + 2|B|^2), \quad (2.7)$$

$$\frac{\partial B}{\partial \tau} = \frac{\partial^2 B}{\partial Y^2} + \delta B - B(|B|^2 + 2|A|^2) \quad (2.8)$$

(see Daniels & Weinstein 1996). Finite values of δ are equivalent to an order- L^{-2} band of values of ϵ above the critical value for an infinite layer, $\epsilon = 0$. Although the scalings (2.4)–(2.6) lead to the absence of Y and X derivatives in (2.7) and (2.8) respectively, both A and B will in general vary with both X and Y through the nonlinear interaction.

Boundary conditions for the system (2.7), (2.8) may be derived from (2.2), (2.3) (Daniels & Weinstein 1996) and are

$$A = 0 \quad \text{at} \quad X = 0 \text{ and } X = 1, \quad (2.9)$$

$$B = 0 \quad \text{at} \quad Y = 0 \text{ and } Y = a, \quad (2.10)$$

where $a = M/L$ is the aspect ratio of the rectangular planform. The absence of conditions on B at $X = 0, 1$ and A at $Y = 0, a$ is consistent with the form of equations (2.7), (2.8) and with the tendency for rolls to align perpendicular to lateral boundaries. The adjustment to the amplitude of this component to accommodate the full boundary conditions (2.2), (2.3) occurs within boundary layers of thickness x (or y) $\sim \epsilon^{-1/4} \sim L^{1/2}$ where fourth-order spatial derivatives enter the amplitude equations. These boundary layers are discussed by Brown & Stewartson (1977) and Daniels & Weinstein (1992) and are generally passive, allowing the amplitude and gradient in amplitude of the rolls to reduce to zero at the boundary.

The system (2.7)–(2.10) also governs Rayleigh–Bénard convection in a rectangular container with rigid horizontal boundaries and either perfectly insulating or perfectly conducting lateral walls, and in this case finite values of δ define an order- L^{-2} band of Rayleigh numbers above the critical value for an infinite layer. Each of the coefficients 2 in equations (2.7), (2.8) is replaced by a Prandtl-number-dependent coefficient whose value varies from 1.23 for infinite Prandtl number to 14.3 for a Prandtl number of zero (Sivapragasam 1995) and for this range of values there is likely to be no qualitative difference in the behaviour of solutions compared with those of (2.7)–(2.10).

Steady-state solutions of (2.7)–(2.10) for A and B are arbitrary to within multiplicative factors $e^{i\alpha}$ and $e^{i\beta}$ respectively, where α and β are functions of Y and X respectively, corresponding to a possible curvature of the rolls. In practice the phase of the solution in the final steady state is expected to emerge on a time scale $t = O(L^3)$ and to be determined by higher-order effects in the expansions in inverse powers of L and matching with the sidewalls in the manner described by Daniels (1978). In the context of the present system, the forms of $\alpha(Y)$ and $\beta(X)$ will be fixed by whatever initial conditions are specified at $\tau = 0$ and so it will be assumed that A and B are real functions of X, Y and τ . For the modes of interest here it can also be assumed that A and B are positive.

3. Solutions for finite δ

One steady-state solution of (2.7)–(2.10) is $A = B = 0$ but this state of no motion becomes unstable when δ exceeds a critical value and convective rolls then develop. If $a < 1$ the primary bifurcation occurs at $\delta = \pi^2$ and consists of x -rolls, so that $B = 0$ and

$$A = \left(\frac{2\delta m}{1+m} \right)^{1/2} \text{sn}(u, m), \quad \delta > \pi^2, \quad (3.1)$$

where $u = (\delta/(m+1))^{1/2}X$ and m is determined from the boundary conditions (2.9) by the relation

$$\delta^{1/2} = 2(1+m)^{1/2}K(m). \quad (3.2)$$

Here sn is the Jacobian elliptic function and K is the complete elliptic integral of the first kind (see for example Abramowitz & Stegun 1965, p. 569). Further bifurcations to x -roll solutions correspond to taking integer multiples of the right-hand side of (3.2) and occur at $\delta = n^2\pi^2$ ($n = 2, 3, \dots$) but these branches are expected to be unstable.

Similarly, steady-state solutions of (2.7)–(2.10) with $A = 0$ and B non-zero (y -rolls) emerge as bifurcations at $\delta = n^2\pi^2/a^2$ ($n = 1, 2, \dots$) and can also be expressed in terms of Jacobian elliptic functions. In practice if $a < 1$ these solutions are of minor significance since the primary solution will already have been established. However, it follows from (2.8) that the solution (3.1) is susceptible to disturbances in the form of y -rolls in the regions near the boundaries $X = 0$ and $X = 1$ where its amplitude falls below $(\delta - \pi^2/a^2)^{1/2}/\sqrt{2}$ and so a secondary bifurcation occurs from the primary branch (3.1) at $\delta = \pi^2/a^2$ in which there is a combination of x -rolls and y -rolls near each shorter side of the rectangle. The detailed structure of the bifurcation is described by Daniels & Weinstein (1996). Near $X = 0$ there is a transition line located at

$$X = X_T \sim (\delta - \pi^2/a^2)^{1/2}S_T(a), \quad \delta \rightarrow \pi^2/a^2+, \quad (3.3)$$

where $S_T(a) = m^{-1/2}\{K(m)\}^{-2}/8$, m being determined by (3.2) with the left-hand side replaced by π/a . This transition line is the grain boundary. For $X < X_T$, both A and B are non-zero and small, with

$$B \approx \frac{2}{\sqrt{3}}(\delta - \pi^2/a^2)^{1/2}\{(S_T^2 - S^2)^{1/2}/S_T\} \sin(\pi Y/a), \quad S < S_T, \quad (3.4)$$

where $S = (\delta - \pi^2/a^2)^{-1/2}X$. For $X_T < X < 1 - X_T$, B is zero and a first approximation to A is given by (3.1) although there is a Y -dependent correction of order $(\delta - \pi^2/a^2)^{5/2}$ generated by the behaviour near the transition line. A second transition line, or grain boundary, is symmetrically placed at $X = 1 - X_T$ near the wall $X = 1$.

Daniels & Weinstein (1996) computed numerical solutions of (2.7)–(2.10) to trace the secondary solution branch for values of δ greater than π^2/a^2 . Their solutions for an aspect ratio $a = 0.6$ show that the grain boundaries move towards the centre of the rectangle initially, reaching $X_T \approx 0.125$ when $\delta \approx 95$ but then start to retreat again at higher values of δ . In the region $X_T < X < 1 - X_T$ the steady-state solution for B is identically zero so that the solution there consists entirely of x -rolls, while the regions $X < X_T$ and $X > 1 - X_T$ contain a combination of x -rolls and y -rolls.

We have now extended the numerical solution to much higher values of δ , in the range $\delta = 200$ to $\delta = 1800$. Solutions were computed from initial distributions

$$A = \sin(\pi X), \quad B = \sin(\pi Y/a) \quad \text{at} \quad \tau = 0 \quad (3.5)$$

using an explicit finite difference scheme. The system was discretized onto a uniform grid in X and Y and allowed to evolve in time to a steady-state solution. As the value of δ increases, the amplitude functions develop rapid variations near the corners and shorter sides of the rectangle and for computations with $a = 0.6$ it was necessary to use grids of up to 160×96 points (equivalent to step lengths $\Delta X = \Delta Y = 0.00625$) in order to maintain reasonable accuracy. Time steps were used consistent with the stability criterion for the corresponding linear diffusion equations, typically $\Delta\tau = 10^{-5}$. Tests were carried out to monitor the convergence of the solution to its steady-state form, and for most cases this was effectively achieved when $\tau \approx 0.6$, a somewhat

smaller value ($\tau \approx 0.4$) being sufficient for the largest values of δ . A cubic spline interpolation was used to monitor the value X_0 of X at which $A = (\delta - \pi^2/a^2)^{1/2}/\sqrt{2}$ on $Y = a/2$. This provides an approximation to the location of the grain boundary and is easier to estimate from the numerical solution than the position at which B falls to zero. Strictly speaking the grain boundary $X = X_T$ can be defined by the largest value of X at which the steady linearized version of (2.8),

$$\frac{\partial^2 B}{\partial Y^2} + (\delta - 2|A|^2)B = 0, \quad (3.6)$$

subject to $B = 0$ at $Y = 0$ and $Y = a$ has a non-trivial eigensolution. If A is independent of Y then this corresponds precisely to the condition $|A| = (\delta - \pi^2/a^2)^{1/2}/\sqrt{2}$ mentioned above. In practice A is not independent of Y at X_T , but this condition remains a good approximation for general values of δ and is correct to leading order both as $\delta \rightarrow \pi^2/a^2$, and (as we shall see later) as $\delta \rightarrow \infty$.

Figures 1–4 show a selection of numerical results obtained for the steady-state solution with $a = 0.6$. Figure 1 shows profiles of A and B as functions of Y for values of X in the region $0 \leq X \leq 0.2$ when $\delta = 200$. The solutions for A and B are symmetric about both $X = \frac{1}{2}$ and $Y = a/2$. Non-zero values of B are restricted to the regions near $X = 0$ and $X = 1$ so that, for example, all of the profiles of B for $0.125 \leq X \leq 0.2$ in figure 1 are zero and the value of X_0 is 0.1152. The profile at $X = 0$ is a Jacobian elliptic function, being the leading mode of the steady-state solution of (2.8) with $A = 0$, subject to $B = 0$ at $Y = 0$ and $Y = a$. Contours of the y -roll amplitude follow curved paths with maximum width at $Y = a/2$ and in this sense the grain boundary will appear to possess curvature, despite the straight line $X = X_T$ associated with (3.6). Contours of the Swift–Hohenberg function ψ reconstructed from (2.4) using a value $L = 30\pi$ are shown in figure 2. This illustrates the effective curvature of the grain boundary and gives a good indication of the complicated roll patterns near the corners and shorter sides of the rectangle. In general, the results are in good agreement with both the full numerical simulations of the Swift–Hohenberg equation by Greenside & Coughran (1984, figure 9) and the experiments of Pocheau & Croquette (1984) although it should be noted that the reconstruction in figure 2 excludes the $L^{1/2}$ boundary layers described in §2.

Results for $\delta = 900$ are shown in figures 3 and 4. As δ increases, the grain boundaries move closer to the walls $X = 0$ and $X = 1$, and the profile of B at $X = 0.075$ in figure 3 clearly indicates the slow growth in amplitude of y -rolls near the sides $Y = 0$ and $Y = a$ as X decreases below X_0 , which for $\delta = 900$ has the value 0.0798. There is a substantial variation in A as a function of Y near $X = X_0$, but nearer the wall $X = 0$ both A and B become relatively independent of Y in the central region, with the main variation now restricted to the corners of the rectangle. The plateau in B at $X = 0$ is a manifestation of the form of the leading-mode Jacobian elliptic function mentioned earlier, in the limit as $\delta \rightarrow \infty$. Figure 4 shows contours of the function ψ for $L = 30\pi$.

4. Boundary-layer structure for large δ

A schematic diagram of the proposed steady-state structure of the solution near $X = 0$ as $\delta \rightarrow \infty$ is shown in figure 5. A key feature is that as X increases from zero the solution for B is assumed to reach exponentially small values along a path

$$X = \delta^{-1/2}U(Y), \quad (4.1)$$

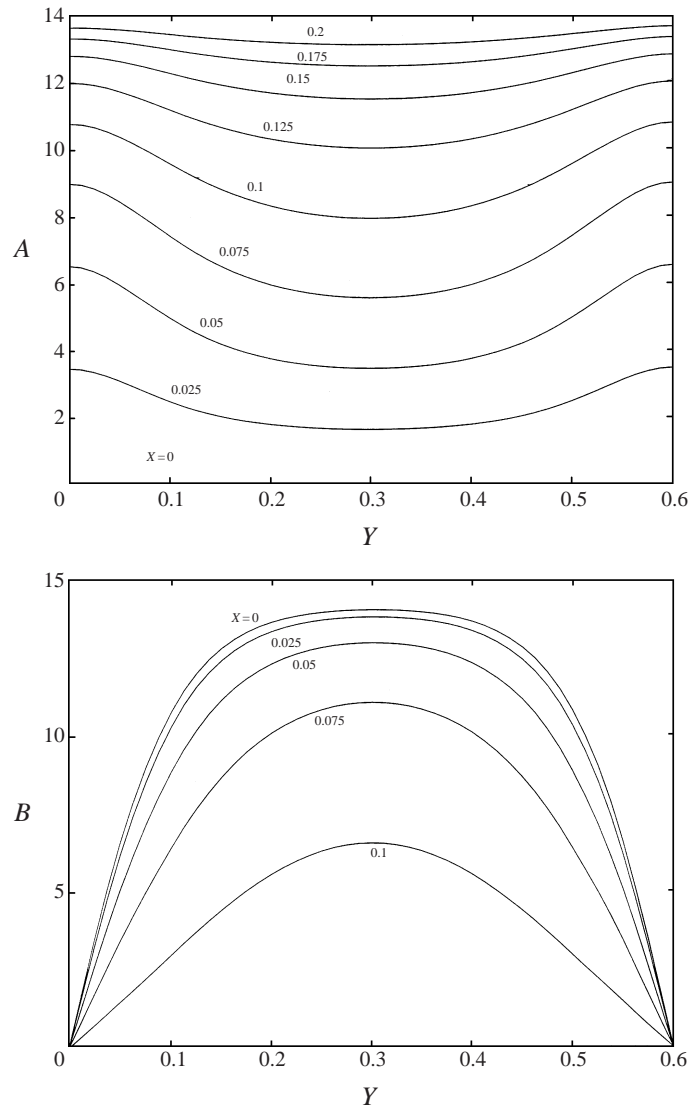


FIGURE 1. Steady-state profiles of A and B as functions of Y at various values of X for the case $a = 0.6$ and $\delta = 200$.

where the function $U(Y)$ is initially unknown, and will be determined as part of the solution. This implies that the *effective* transition line, or grain boundary, is located at $X = \delta^{-1/2}U(Y)$ rather than at $X = X_T$, the solution of (3.6). With $X_T = \delta^{-1/2}U(a/2)$, the solution for B bifurcates from zero at $X = X_T$ but remains exponentially small in the region $\delta^{-1/2}U(Y) < X < X_T$. The bifurcation at X_T is 'local' in the sense that the eigenfunction of (3.6) is non-exponentially small only in the immediate neighbourhood of $Y = a/2$.

In (4.1) it will emerge subsequently that U itself must be expanded in logarithmic functions of δ but for the purposes of the analysis it may be viewed initially as an order-one function of Y ; the basic boundary-layer scaling of $\delta^{-1/2}$ for X is suggested by the balance of the spatial derivative in (2.7).

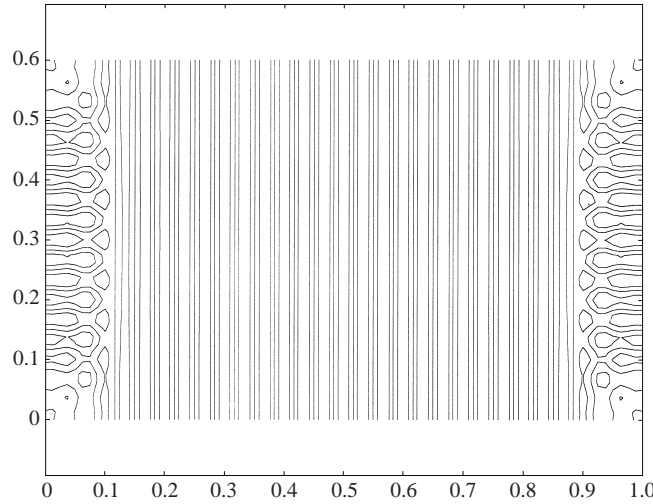


FIGURE 2. Steady-state contours of ψ with $L = 30\pi$ for the case $a = 0.6$ and $\delta = 200$.

The main boundary-layer structure is now formulated using the coordinate transformation $(X, Y) \rightarrow (s, Y)$ where $X = \delta^{-1/2}(s + U(Y))$ so that A and B satisfy

$$\delta \frac{\partial^2 A}{\partial s^2} + \delta A = A^3 + 2AB^2, \tag{4.2}$$

$$\left(\frac{\partial}{\partial Y} - U' \frac{\partial}{\partial s} \right)^2 B + \delta B = B^3 + 2BA^2, \tag{4.3}$$

where $U' = dU/dY$.

In the outer region of the boundary layer where $s > 0$ (region II in figure 5) it is assumed that $B = 0$ (to within exponentially small order) and

$$A = \delta^{1/2} A_0(s, Y) + \delta^{-1/2} A_1(s, Y) + \dots \tag{4.4}$$

Substitution into (4.2) gives

$$\frac{\partial^2 A_0}{\partial s^2} + A_0(1 - A_0^2) = 0 \tag{4.5}$$

and matching with the core region (region I in figure 5) where $A \sim \delta^{1/2}$ requires $A_0 \rightarrow 1$ as $s \rightarrow \infty$. It follows that

$$A_0 = \tanh \left\{ (s + c)/\sqrt{2} \right\}, \quad s > 0, \tag{4.6}$$

where $c = c(Y)$.

In the inner region of the boundary layer where $s < 0$ (region IV in figure 5) the expansion (4.4) is still appropriate for A and now

$$B = \delta^{1/2} B_0(s, Y) + \delta^{-1/2} B_1(s, Y) + \dots \tag{4.7}$$

Substitution into (4.2) and (4.3) gives

$$B_0^2 = 1 - 2A_0^2 \tag{4.8}$$

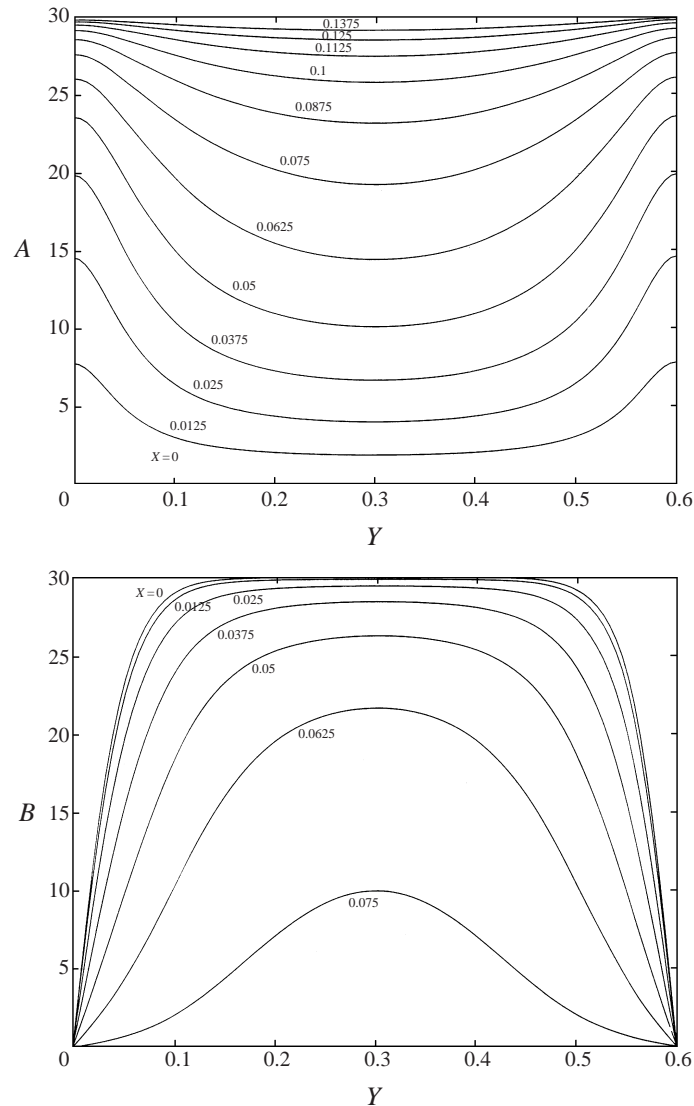


FIGURE 3. Steady-state profiles of A and B as functions of Y at various values of X for the case $a = 0.6$ and $\delta = 900$.

and

$$\frac{\partial^2 A_0}{\partial s^2} + (3A_0^2 - 1)A_0 = 0. \tag{4.9}$$

Since it is required that $B_0 \rightarrow 0$ as $s \rightarrow 0^-$ it follows from (4.8) that $A_0 = 1/\sqrt{2}$ at $s = 0$ and if A_0 is continuous at $s = 0$ then $c = \sqrt{2} \tanh^{-1}(1/\sqrt{2})$. Thus $A_0(s, Y)$ is independent of Y in $s > 0$. Assuming $\partial A_0/\partial s$ is also continuous at $s = 0$, the solution of (4.9) must now satisfy $A_0 = 1/\sqrt{2}, \partial A_0/\partial s = 1/(2\sqrt{2})$ at $s = 0^-$ and so is given by

$$A_0 = \sqrt{2/3} \operatorname{sech}(d - s), \tag{4.10}$$

where $d = \ln(\sqrt{3})$. Thus $A_0(s, Y)$ is also independent of Y in $s < 0$. An immediate

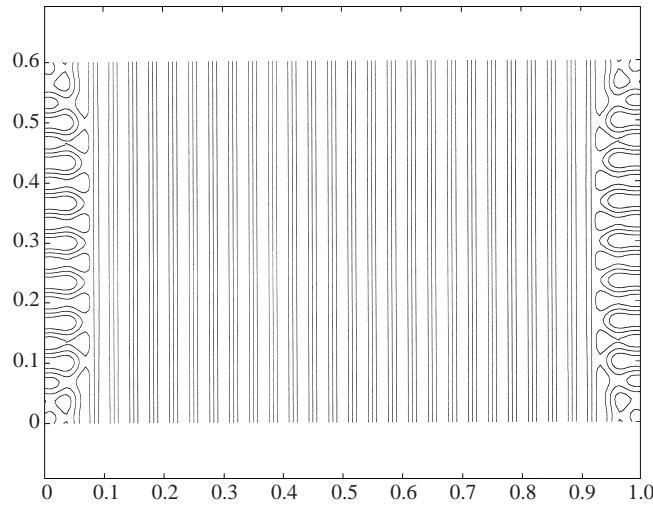


FIGURE 4. Steady-state contours of ψ with $L = 30\pi$ for the case $a = 0.6$ and $\delta = 900$.

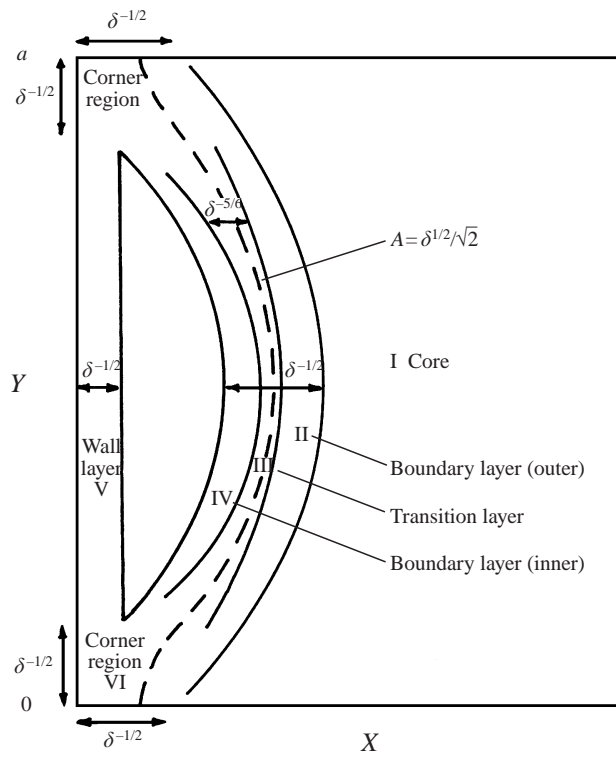


FIGURE 5. Schematic diagram of the main regions involved in the asymptotic structure of the solution as $\delta \rightarrow \infty$.

consequence of the result (4.10) is that A_0 is positive for all $s < 0$ and so the boundary condition $A = 0$ cannot be satisfied at a finite value of s . Instead, the exponential behaviour

$$A_0 \sim 2\sqrt{2}e^s/3, \quad B_0 \sim 1 - 8e^{2s}/9 \quad \text{as } s \rightarrow -\infty \quad (4.11)$$

suggests that the whole boundary layer must sit away from the wall, equivalent to the function U in (4.1) containing a component which is large as $\delta \rightarrow \infty$. This result could be anticipated from the boundary-layer analysis of Daniels & Weinstein (1992) which showed that for an isolated wall with no Y -dependence and $A = \lambda$ at $X = 0$ in place of (2.9), the grain boundary moves away from the wall as $\lambda \rightarrow 0$. In the present situation it is therefore the Y -dependence of the solution that must allow the grain boundary to achieve an equilibrium position. This enters the boundary-layer solution through the correction terms A_1 and B_1 in (4.4) and (4.7).

In $s > 0$, A_1 satisfies

$$\frac{\partial^2 A_1}{\partial s^2} + A_1(1 - 3A_0^2) = 0, \quad (4.12)$$

with $A_1 \rightarrow 0$ as $s \rightarrow \infty$ and so

$$A_1 = c_1 \frac{\partial A_0}{\partial s} = \frac{c_1}{\sqrt{2}} \operatorname{sech}^2 \{(s+c)/\sqrt{2}\}, \quad (4.13)$$

where $c_1 = c_1(Y)$.

In $s < 0$, it is found that

$$B_1 = -2A_0A_1B_0^{-1} + \frac{1}{2}U'^2B_0^{-2}\frac{\partial^2 B_0}{\partial s^2} - \frac{1}{2}U''B_0^{-2}\frac{\partial B_0}{\partial s}, \quad (4.14)$$

where A_1 satisfies

$$\frac{\partial^2 A_1}{\partial s^2} + A_1(9A_0^2 - 1) = 2A_0B_0^{-1} \left(U'^2 \frac{\partial^2 B_0}{\partial s^2} - U'' \frac{\partial B_0}{\partial s} \right). \quad (4.15)$$

The general solution is

$$A_1 = (d_1 + d_2Q(s) + U'^2Q_1(s) + U''Q_2(s)) \frac{\partial A_0}{\partial s}, \quad (4.16)$$

where $d_{1,2} = d_{1,2}(Y)$ are associated with the two complementary solutions and

$$Q(s) = \frac{3}{2}s - \frac{5}{3} + \coth(d-s) - \frac{1}{4} \sinh \{2(d-s)\}. \quad (4.17)$$

The functions Q_1 and Q_2 involved in the particular solutions are

$$Q_1(s) = \ln \{4(v-1)/(3(v+1))\} \quad (4.18)$$

and

$$Q_2(s) = \frac{3}{4} \int_1^v (1 - v^2/4)^{-2} v^{-2} H(v) dv, \quad (4.19)$$

where

$$H(v) = 2v - \frac{20}{9} - \frac{2}{9}v^3 + \ln \{3(v-1)/(v+1)\} \quad (4.20)$$

and $v = 2 \tanh(d-s)$. The dominant behaviour of the solution for A_1 as $s \rightarrow -\infty$ is associated with the second complementary solution, which is exponentially large, so that

$$A_1 \sim -d_2 e^{-s}/(2\sqrt{2}), \quad s \rightarrow -\infty. \quad (4.21)$$

In order to determine the function d_2 the solutions in the inner and outer regions of the boundary layer must be matched across the transition layer at $s = 0$. From the preceding results it follows that as $s \rightarrow 0+$,

$$A = \frac{\delta^{1/2}}{\sqrt{2}} \left\{ 1 + \frac{1}{2}s - \frac{1}{4}s^2 + \frac{1}{24}s^3 + \frac{1}{48}s^4 + \dots \right\} + \frac{\delta^{-1/2}}{2\sqrt{2}} \{c_1 - c_1s + \dots\} + \dots \quad (4.22)$$

and as $s \rightarrow 0-$,

$$\begin{aligned}
 A = & \frac{\delta^{1/2}}{\sqrt{2}} \left\{ 1 + \frac{1}{2}s - \frac{1}{4}s^2 - \frac{7}{24}s^3 - \frac{1}{48}s^4 + \dots \right\} \\
 & + \frac{\delta^{-1/2}}{2\sqrt{2}} \left\{ U^2 \ln(-s) + d_1 - (U^2 + 2U'')s \ln(-s) \right. \\
 & \left. + \left(\frac{16}{3}d_2 - d_1 + \frac{5}{4}U^2 + 2U''\left(\frac{13}{9} + \ln \frac{4}{9}\right)\right)s + \dots \right\} + \dots, \tag{4.23}
 \end{aligned}$$

$$B = \delta^{1/2}(-s)^{1/2} + \dots . \tag{4.24}$$

These results suggest the form which the solution must take in the transition layer, which is considered next.

5. Transition layer

The width of the transition layer (region III in figure 5) is dictated by the need for the second-order spatial derivative of B with respect to s to appear at leading order in equation (4.3). This requires $B \sim s^{-1} \sim \delta^{1/3}$ and the expansions (4.22)–(4.24) suggest that locally A and B should be expanded in the form

$$A = \delta^{1/2}\tilde{A}_0 + \delta^{1/6}\tilde{A}_1 + \delta^{-1/6}\tilde{A}_2 + \delta^{-1/2}\tilde{A}_3 + \delta^{-5/6}\tilde{A}_4 + \dots, \tag{5.1}$$

$$B = \delta^{1/3}\tilde{B}_0 + \tilde{B}_1 + \dots, \tag{5.2}$$

where \tilde{A}_i and \tilde{B}_i are functions of \tilde{s} and Y , and $s = \delta^{-1/3}\tilde{s}$. Substitution into (4.2) and matching with (4.22) and (4.23) gives in succession

$$\tilde{A}_0 = 1/\sqrt{2}, \quad \tilde{A}_1 = \tilde{s}/(2\sqrt{2}), \quad \tilde{A}_2 = -\tilde{s}^2/(4\sqrt{2}). \tag{5.3}$$

Also the solutions for \tilde{A}_3 and \tilde{A}_4 may be written in the form

$$\tilde{A}_3 = \tilde{s}^3/(24\sqrt{2}) + \sqrt{2} \int_{\tilde{s}}^{\infty} \int_{\tilde{s}}^{\infty} \tilde{B}_0^2 d\tilde{s} d\tilde{s} + \alpha_3\tilde{s} + \beta_3, \tag{5.4}$$

$$\tilde{A}_4 = \tilde{s}^4/(48\sqrt{2}) + (1/\sqrt{2}) \int_{\tilde{s}}^{\infty} \int_{\tilde{s}}^{\infty} (\tilde{s}\tilde{B}_0^2 + 4\tilde{B}_0\tilde{B}_1) d\tilde{s} d\tilde{s} + \alpha_4\tilde{s} + \beta_4, \tag{5.5}$$

where $\alpha_{3,4}$ and $\beta_{3,4}$ are functions of Y . From (4.3), \tilde{B}_0 satisfies the equation

$$U'^2 \frac{\partial^2 \tilde{B}_0}{\partial \tilde{s}^2} - \tilde{s}\tilde{B}_0 - \tilde{B}_0^3 = 0 \tag{5.6}$$

and a solution is required for which $\tilde{B}_0 \rightarrow 0$ as $\tilde{s} \rightarrow \infty$ and, from (4.24), $\tilde{B}_0 \sim (-\tilde{s})^{1/2}$ as $\tilde{s} \rightarrow -\infty$. This can be written in the form

$$\tilde{B}_0 = |U'|^{1/3} f_0(\xi), \tag{5.7}$$

where $\xi = |U'|^{-2/3} \tilde{s}$ and f_0 is a scaled form of the second Painleve transcendent satisfying

$$f_0'' - \xi f_0 - f_0^3 = 0, \quad f_0 \rightarrow 0 \quad (\xi \rightarrow \infty), \quad f_0 \sim (-\xi)^{1/2} \quad (\xi \rightarrow -\infty), \tag{5.8}$$

and whose properties are discussed by Rosales (1978) in the context of its relevance in a similarity solution of the Korteweg–de Vries equation and also by Miles (1978).

Note that the modulus is used in (5.7) in anticipation of the fact that U' is negative for $Y > a/2$. Indeed, symmetry implies that $U' = 0$ at $Y = a/2$ so that the width of the transition layer approaches zero there. This is consistent with the abrupt growth of B from zero in the immediate neighbourhood of $Y = a/2, X = X_T$, in line with the 'local' bifurcation structure mentioned at the start of §4. The details of the local solution, which is expected to be passive, are not given here. The solution for f_0 is exponentially small as $\xi \rightarrow \infty$ and has the asymptotic form

$$f_0 \sim (-\xi)^{1/2} - (-\xi)^{-5/2}/8 + O((-\xi)^{-11/2}), \quad \xi \rightarrow -\infty. \tag{5.9}$$

The double integral appearing in the solution (5.4) for \tilde{A}_3 can now be calculated in terms of f_0 . One integration gives

$$\int_{\tilde{s}}^{\infty} \tilde{B}_0^2 d\tilde{s} = |U'|^{4/3} I_1(\xi), \tag{5.10}$$

where

$$I_1(\xi) = f_0'^2 - \xi f_0^2 - \frac{1}{2} f_0^4 \sim \frac{1}{2} \xi^2 - \frac{1}{4} \xi^{-1} + O(\xi^{-4}), \quad \xi \rightarrow -\infty. \tag{5.11}$$

Note that I_1 contains no finite part as $\xi \rightarrow -\infty$. A further integration then gives

$$\int_{\tilde{s}}^{\infty} \int_{\tilde{s}}^{\infty} \tilde{B}_0^2 d\tilde{s} d\tilde{s} = U'^2 I_2(\xi), \tag{5.12}$$

where, for $\xi < 0$,

$$I_2(\xi) = \frac{1}{4} \ln(-\xi) - \frac{1}{3} \xi I_1(\xi) + \frac{1}{3} f_0 f_0' + I_0(\xi) \tag{5.13}$$

and

$$I_0(\xi) = \int_{-1}^{\infty} f_0'^2 d\xi + \int_{\xi}^{-1} (f_0'^2 - \frac{1}{4}(-\xi)^{-1}) d\xi \rightarrow k \text{ as } \xi \rightarrow -\infty, \tag{5.14}$$

where the value of k can be obtained from a numerical solution of (5.8) but will not be needed explicitly here. Thus

$$I_2 \sim -\frac{1}{6} \xi^3 + \frac{1}{4} \ln(-\xi) + k - \frac{1}{12} + o(1), \quad \xi \rightarrow -\infty. \tag{5.15}$$

It now follows from (5.4) that

$$\tilde{A}_3 \sim \tilde{s}^3 / (24\sqrt{2}) + \alpha_3 \tilde{s} + \beta_3, \quad \tilde{s} \rightarrow \infty \tag{5.16}$$

and

$$\tilde{A}_3 \sim -7\tilde{s}^3 / (24\sqrt{2}) + \alpha_3 \tilde{s} + U'^2 (\ln(-|U'|^{-2/3} \tilde{s}) + 4k - \frac{1}{3}) / (2\sqrt{2}) + \beta_3, \quad \tilde{s} \rightarrow -\infty. \tag{5.17}$$

The equation for \tilde{B}_1 is

$$U'^2 \frac{\partial^2 \tilde{B}_1}{\partial \tilde{s}^2} - \tilde{s} \tilde{B}_1 - 3\tilde{B}_0^2 \tilde{B}_1 = \left(U'' + 2U' \frac{\partial}{\partial Y} \right) \frac{\partial \tilde{B}_0}{\partial \tilde{s}} - \frac{1}{4} \tilde{s}^2 \tilde{B}_0 \tag{5.18}$$

and the solution can be written

$$\tilde{B}_1 = |U'| f_1(\xi) + U'' |U'|^{-1} f_2(\xi), \tag{5.19}$$

where f_1 and f_2 satisfy

$$f_1'' - \xi f_1 - 3f_0^2 f_1 = -\frac{1}{4} \xi^2 f_0, \tag{5.20}$$

$$f_2'' - \xi f_2 - 3f_0^2 f_2 = \frac{1}{3} f_0' - \frac{4}{3} \xi f_0'', \tag{5.21}$$

with boundary conditions requiring that $f_{1,2} \rightarrow 0$ as $\xi \rightarrow \infty$ and that $f_{1,2}$ are not exponentially large as $\xi \rightarrow -\infty$. It now follows that in the solution for \tilde{A}_4 the integral

$$\int_{\tilde{s}}^{\infty} \tilde{B}_0 \tilde{B}_1 d\tilde{s} = U'^2 I_{31}(\xi) + U'' I_{32}(\xi), \quad (5.22)$$

where

$$I_{31}(\xi) = f_0' f_1' - f_0^3 f_1 - \xi f_0 f_1 + \frac{1}{8} \xi^2 f_0^2 + \frac{1}{4} \xi I_1(\xi) + \frac{1}{4} I_2(\xi) \quad (5.23)$$

and, for $\xi < 0$,

$$I_{32}(\xi) = f_0' f_2' - \xi f_0 f_2 - f_0^3 f_2 + \frac{1}{4} \ln(-\xi) + I_0(\xi) + \frac{2}{3} \xi f_0'^2. \quad (5.24)$$

The other integral appearing in the solution for \tilde{A}_4 is

$$\int_{\tilde{s}}^{\infty} \tilde{s} \tilde{B}_0^2 d\tilde{s} = U'^2 I_4(\xi) \quad (5.25)$$

where

$$I_4(\xi) = \xi I_1(\xi) + I_2(\xi). \quad (5.26)$$

Making use of the limiting forms (5.11), (5.14) and (5.15) it now follows that

$$\tilde{A}_4 \sim \tilde{s}^4 / (48\sqrt{2}) + \alpha_4 \tilde{s}, \quad \tilde{s} \rightarrow \infty \quad (5.27)$$

and

$$\begin{aligned} \tilde{A}_4 \sim & -\tilde{s}^4 / (48\sqrt{2}) - (U'^2 + 2U'')(\tilde{s} \ln(-|U'|^{-2/3} \tilde{s})) / (2\sqrt{2}) \\ & + (\alpha_4 - \sqrt{2}(U'^2(k - \frac{19}{48}) + 2U''(k - \frac{5}{12})))\tilde{s}, \quad \tilde{s} \rightarrow -\infty. \end{aligned} \quad (5.28)$$

It is now possible to match the transition-layer solution (5.1) as $\tilde{s} \rightarrow \infty$ with the outer boundary-layer solution (4.22) as $s \rightarrow 0+$, yielding $\alpha_3 = 0$ and

$$c_1 = 2\sqrt{2}\beta_3 = -2\sqrt{2}\alpha_4, \quad (5.29)$$

and the transition-layer solution as $\tilde{s} \rightarrow -\infty$ with the inner boundary-layer solution (4.23) as $s \rightarrow 0-$, yielding $\alpha_3 = 0$ and

$$d_1 = U'^2(\frac{1}{3} \ln \delta - \frac{2}{3} \ln |U'| + 4k - \frac{1}{3}) + 2\sqrt{2}\beta_3, \quad (5.30)$$

$$\begin{aligned} & -d_1 + \frac{16}{3}d_2 + \frac{5}{4}U'^2 + 2U''(\frac{13}{9} + \ln \frac{4}{9}) \\ & = 2\sqrt{2}\alpha_4 - (U'^2 + 2U'')(\frac{1}{3} \ln \delta - \frac{2}{3} \ln |U'| + 4k) + \frac{1}{12}(19U'^2 + 40U''). \end{aligned} \quad (5.31)$$

The key result is now obtained by adding (5.30) and (5.31) and making use of (5.29) to obtain

$$8d_2 = U''(2 \ln |U'| - \ln \delta - k_2), \quad (5.32)$$

where $k_2 = 12k + 3 \ln \frac{4}{9} - \frac{2}{3}$. It should be noted that d_2 is not finite as $\delta \rightarrow \infty$ since it contains the term $-\frac{1}{8}U'' \ln \delta$ (and it will emerge that U'' is finite as $\delta \rightarrow \infty$). This in turn implies that the boundary-layer correction term A_1 contains a contribution of order $\ln \delta$ as $\delta \rightarrow \infty$. This does not invalidate the determination of A_1 since logarithmic adjustments do not introduce any new effects into its governing equation.

The result (5.32) implies that the effect of the transition layer is to generate the component of A_1 in $s < 0$ which is exponentially large as $s \rightarrow -\infty$. This behaviour must be consistent with the solution in the wall layer, which is considered next.

6. Wall layer and location of the grain boundary

From (4.11) and (4.21) the solution in the inner region of the boundary layer has the form

$$A \sim \delta^{1/2}\{2\sqrt{2}e^s/3 + \dots\} - \delta^{-1/2}\{d_2e^{-s}/(2\sqrt{2}) + \dots\} + \dots \quad (6.1)$$

as $s \rightarrow -\infty$. This generates a solution in the wall layer (region IV in figure 5) where the local coordinate \bar{X} is defined by $X = \delta^{-1/2}\bar{X}$. Here the untransformed version of the governing equations is used. The relevant leading-order solution of (2.8) is $B = \delta^{1/2}$ and since $A = \bar{G}(\bar{X}, Y) + \dots$ is small compared with $\delta^{1/2}$ it satisfies the linearized version of (2.7), namely

$$\frac{\partial^2 \bar{G}}{\partial \bar{X}^2} - \bar{G} = 0. \quad (6.2)$$

Since $\bar{G} = 0$ on $\bar{X} = 0$ it follows that

$$\bar{G} = G(Y) \sinh \bar{X} \quad (6.3)$$

and since $\bar{X} = s + U$, matching with (6.1) as $\bar{X} \rightarrow \infty$ implies that

$$G = 4\sqrt{2}\delta^{1/2}e^{-U}/3 = d_2\delta^{-1/2}e^{U/\sqrt{2}}. \quad (6.4)$$

The wall effectively reflects the incoming exponential component in A_0 to produce the outgoing exponential component in A_1 ; the position of the grain boundary must be such that this reflection is of the correct size to counterbalance the generation of d_2 by the transition layer. Substitution for d_2 from (5.32) in (6.4) implies that U satisfies

$$U''(2 \ln |U'| - \ln \delta - k_2) = 64\delta e^{-2U}/3. \quad (6.5)$$

Writing

$$U = \frac{1}{2} \ln \delta - \frac{1}{2} \ln(\ln \delta) + P(Y), \quad (6.6)$$

it follows that $P(Y)$ satisfies

$$P'' + 64e^{-2P}/3 = (\ln \delta)^{-1}F(P', P''), \quad (6.7)$$

where

$$F(P', P'') = P''(2 \ln |P'| - k_2). \quad (6.8)$$

This suggests that P can now be expanded in inverse powers of $\ln \delta$,

$$P = \bar{P}_0(Y) + (\ln \delta)^{-1}P_1(Y) + \dots, \quad (6.9)$$

where the leading term P_0 satisfies the equation

$$P_0'' + 64e^{-2P_0}/3 = 0. \quad (6.10)$$

Assuming the grain boundary to be symmetric, a solution is required for which $P_0' = 0$ at $Y = a/2$. The equation (6.10) admits singularities of the form $P_0 \sim \ln(8 | Y - Y_0 | / \sqrt{3})$, $Y \rightarrow Y_0$, and the second boundary condition requires that such singularities coincide with the sides of the rectangle $Y = 0, a$ so that $P_0 \rightarrow -\infty$ as $Y \rightarrow 0$ and $Y \rightarrow a$. This ensures that the grain boundary approaches the corner regions of the rectangle, to be considered in §7 below. The alternatives are that either singularities occur inside the region $0 < Y < a$, which seems inconsistent with the secondary branch obtained numerically in figures 1–4, or that the grain boundary intersects the boundaries $Y = 0$ and $Y = a$ at a distance of order $\frac{1}{2}\delta^{-1/2} \ln \delta$ from $X = 0$. This latter option is also unreasonable because it would imply a boundary-layer structure along

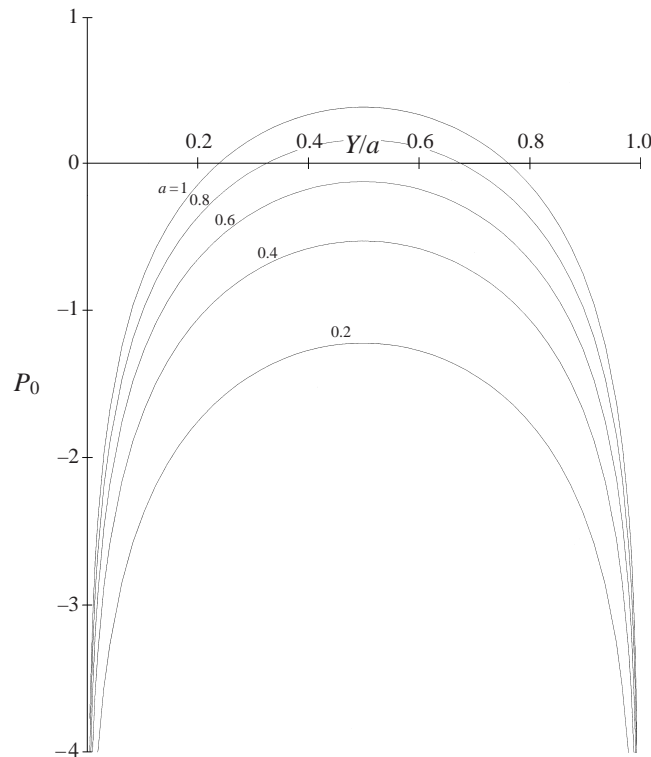


FIGURE 6. Profiles of the grain boundary function $P_0(Y)$ for different values of a .

the walls $Y = 0$ and $Y = a$ which would be unstable to x -rolls. More conclusively, the Jacobian elliptic function (3.1) is actually valid for all δ on $Y = 0$ (since $B = 0$ there) and shows that the contour $A = (\delta/2)^{1/2}$ must intersect the boundary $Y = 0$ at a distance of order $\delta^{-1/2}$ from the corner. The relevant solution of (6.10) is therefore

$$P_0 = \ln(\{8a \sin(\pi Y/a)\}/\{\sqrt{3}\pi\}). \quad (6.11)$$

Profiles of P_0 for different values of the aspect ratio a are shown in figure 6, indicating that the maximum distance of the grain boundary from the wall occurs at $Y = a/2$ and that this distance increases as a increases. From (6.6) the grain boundary is located at

$$X = \delta^{-1/2} \left(\frac{1}{2} \ln \delta - \frac{1}{2} \ln(\ln \delta) + \ln(\{8a \sin(\pi Y/a)\}/\{\sqrt{3}\pi\}) + O((\ln \delta)^{-1}) \right), \quad (6.12)$$

as $\delta \rightarrow \infty$. Figure 7 shows a comparison of the asymptotic formula (6.12) evaluated at $Y = a/2$ with the numerical results reported in §3 for $a = 0.6$. It should be recalled that the numerical results correspond to the value of X at which $A = (\delta - \pi^2/a^2)^{1/2}/\sqrt{2}$ at $Y = a/2$, but from the first two terms of the solution given by (5.1), (5.3) it is clear that this corresponds to the point $\tilde{s} = 0$ within the transition layer, so that the comparison is meaningful. Although numerical solutions were computed for values of δ up to 1800, the values of X_0 obtained for $\delta > 900$ indicate slight deviations as the ability of the numerical grid to accurately resolve the solution worsens. In general, the agreement between the numerical results and the asymptotic formula (6.12) is excellent.

It remains to confirm that the above structure matches with consistent solutions

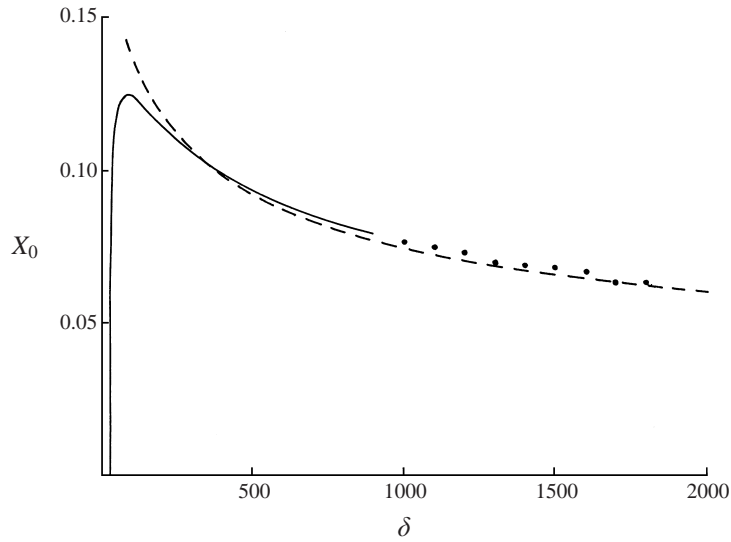


FIGURE 7. The location of the grain boundary as a function of δ for the case $a = 0.6$, showing the steady-state numerical computation of X_0 ($-\cdot\cdot\cdot$) and the asymptotic form given by (6.12) at $Y = a/2$ ($----$).

in the corners of the rectangle. The expansion (6.12) fails when $Y \sim \delta^{-1/2}$ since the third term is then comparable with the first, suggesting that the grain boundary enters a corner region where both X and Y are of order $\delta^{-1/2}$. This is further supported by the fact that the width of the transition layer (region III) is given by $s \sim \delta^{-1/3} |U'|^{2/3} \sim \delta^{-1/3} Y^{-2/3}$ as $Y \rightarrow 0$, so this widens as it enters the corner region and also adopts the scale $s \sim 1$ (equivalent to $X \sim \delta^{-1/2}$) when $Y \sim \delta^{-1/2}$.

7. Corner region

In the corner region at $X = Y = 0$ (region VI in figure 5) it is assumed that

$$A = \delta^{1/2} \bar{A}(\bar{X}, \bar{Y}, \bar{\tau}) + \dots, \quad B = \delta^{1/2} \bar{B}(\bar{X}, \bar{Y}, \bar{\tau}) + \dots, \quad (7.1)$$

where $X = \delta^{-1/2} \bar{X}$, $Y = \delta^{-1/2} \bar{Y}$ and $\tau = \delta^{-1} \bar{\tau}$. The steady-state solution in this region is of primary interest here but time-dependence is retained in anticipation of carrying out a numerical investigation of the solution. Substitution into (2.7), (2.8) shows that \bar{A} and \bar{B} satisfy the full system of equations

$$\frac{\partial \bar{A}}{\partial \bar{\tau}} = \frac{\partial^2 \bar{A}}{\partial \bar{X}^2} + \bar{A} - \bar{A}(\bar{A}^2 + 2\bar{B}^2), \quad (7.2)$$

$$\frac{\partial \bar{B}}{\partial \bar{\tau}} = \frac{\partial^2 \bar{B}}{\partial \bar{Y}^2} + \bar{B} - \bar{B}(\bar{B}^2 + 2\bar{A}^2), \quad (7.3)$$

and a solution is required for which

$$\bar{A} = 0 \quad \text{at} \quad \bar{X} = 0, \quad \bar{B} = 0 \quad \text{at} \quad \bar{Y} = 0, \quad (7.4)$$

$$\bar{A} \rightarrow 1 \quad \text{as} \quad \bar{X} \rightarrow \infty, \quad (7.5)$$

$$\bar{B} \rightarrow (1 - 2\bar{A}^2)^{1/2} \quad (\bar{A} < 1/\sqrt{2}), \quad \bar{B} \rightarrow 0 \quad (\bar{A} > 1/\sqrt{2}) \quad \text{as} \quad \bar{Y} \rightarrow \infty. \quad (7.6)$$

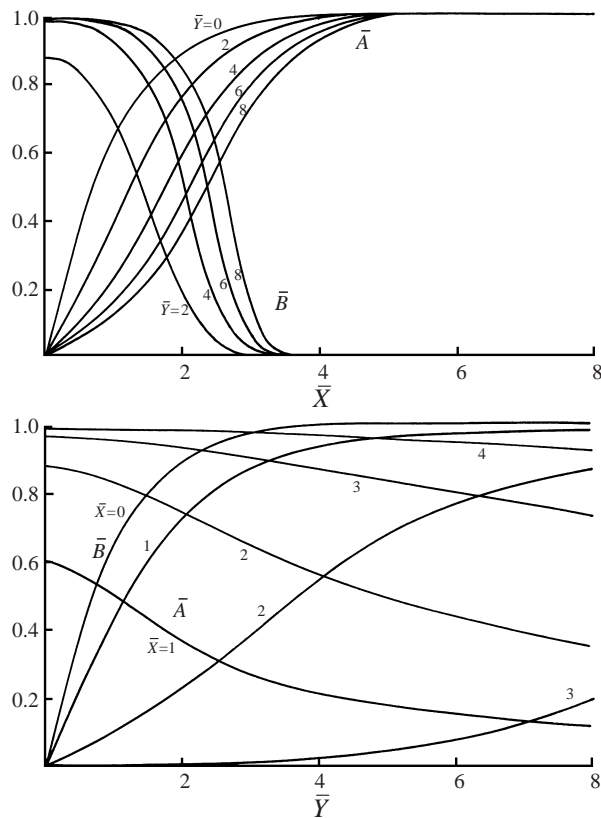


FIGURE 8. Steady-state profiles of \bar{A} and \bar{B} in the corner region.

Numerical solutions were computed using the explicit finite difference scheme of §3 but now in a domain $0 \leq \bar{X} \leq \bar{X}_\infty, 0 \leq \bar{Y} \leq \bar{Y}_\infty$ with the conditions (7.5) and (7.6) applied at the outer boundaries $\bar{X} = \bar{X}_\infty$ and $\bar{Y} = \bar{Y}_\infty$ respectively. An initial state

$$\bar{A} = \sin \{ \pi \bar{X} / (2\bar{X}_\infty) \}, \quad \bar{B} = e^{-\bar{X}} \sin \{ \pi \bar{Y} / (2\bar{Y}_\infty) \} \quad \text{at } \bar{\tau} = 0 \quad (7.7)$$

was used and computations were carried out for various outer boundaries up to $\bar{X}_\infty = 16$ and $\bar{Y}_\infty = 32$, mostly with step lengths $\Delta \bar{X} = 0.2$ and $\Delta \bar{Y} = 0.2$ and 0.4. Convergence to a steady state generally required $\bar{\tau}$ to reach values of up to 600. Steady-state profiles of \bar{A} and \bar{B} in the corner region are shown in figure 8, and figure 9 shows the path of the steady-state contour $\bar{A} = 1/\sqrt{2}$. This provides a good approximation to the line along which \bar{B} reaches exponentially small values in the corner region, especially for large values of \bar{Y} . It intersects the boundary $\bar{Y} = 0$ at $\bar{X} = 1.246$, since the relevant steady-state solution of (7.2) when $\bar{B} = 0$ is $\bar{A} = \tanh(\bar{X}/\sqrt{2})$.

The asymptotic form of the contour $\bar{A} = 1/\sqrt{2}$ as $\bar{Y} \rightarrow \infty$ is also shown in figure 9. This is derived from the governing system (7.2)–(7.6) but the analysis is effectively equivalent to that of §§4–6 with δ replaced by 1 and so only the main properties of the solution are summarized here. The contour is assumed to follow the curve $\bar{X} = \bar{U}(\bar{Y})$ and the asymptotic solution constructed in three regions as $\bar{Y} \rightarrow \infty$: outer ($\bar{s} > 0$), transitional ($\bar{s} \approx 0$) and inner ($\bar{s} < 0$) where $\bar{s} = \bar{X} - \bar{U}(\bar{Y})$, and which correspond to regions II, III and IV outside the corner zone. Working on the assumption that \bar{U}^2

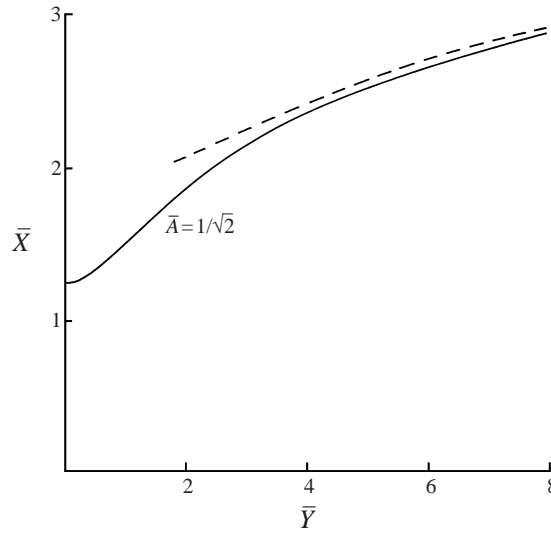


FIGURE 9. Steady-state contour $\bar{A} = 1/\sqrt{2}$ in the corner region, together with the asymptote given by (7.18).

and \bar{U}'' are small and of comparable magnitude as $\bar{Y} \rightarrow \infty$ (to be confirmed below) the inner and outer solutions can be expanded as

$$\bar{A} = \bar{A}_0(\bar{s}) + \{\bar{U}''\bar{A}_{11} + \bar{U}''\bar{A}_{12}\} + \dots, \tag{7.8}$$

with $\bar{B} = 0$ for $\bar{s} > 0$ and

$$\bar{B} = \bar{B}_0(\bar{s}) + \{\bar{U}''\bar{B}_{11} + \bar{U}''\bar{B}_{12}\} + \dots \tag{7.9}$$

for $\bar{s} < 0$. Then for $\bar{s} > 0$

$$\bar{A}_0 = \tanh\{(\bar{s} + c)/\sqrt{2}\}, \quad \bar{A}_{1i} = c_{1i} \frac{\partial \bar{A}_0}{\partial \bar{s}} \quad (i = 1, 2), \tag{7.10}$$

where c is as defined in §4 and c_{1i} are independent of \bar{s} , and for $\bar{s} < 0$

$$\bar{A}_0 = \sqrt{2/3} \operatorname{sech}(d - \bar{s}), \quad \bar{B}_0 = (1 - 2\bar{A}_0^2)^{1/2}, \tag{7.11}$$

$$\bar{A}_{11} = \{d_{11} + d_{21}Q(\bar{s}) + Q_1(\bar{s})\} \frac{\partial \bar{A}_0}{\partial \bar{s}}, \tag{7.12}$$

$$\bar{A}_{12} = \{d_{12} + d_{22}Q(\bar{s}) + Q_2(\bar{s})\} \frac{\partial \bar{A}_0}{\partial \bar{s}}, \tag{7.13}$$

where d, Q, Q_1 and Q_2 are as defined in §4 and d_{ij} are independent of \bar{s} .

The transition layer at $\bar{s} = 0$ is defined by $-\infty < \xi < \infty$ where $\bar{s} = \bar{U}''^{2/3}\xi$ and, anticipating that \bar{U}' is small, is a region of diminishing width as $\bar{Y} \rightarrow \infty$. Locally

$$\bar{B} = \bar{U}'^{1/3}f_0(\xi) + \{\bar{U}'f_1(\xi) + \bar{U}'^{-1}\bar{U}''f_2(\xi)\} + \dots, \tag{7.14}$$

where f_0, f_1 and f_2 are the functions defined in §5. Matching between the inner and outer regions and the transition layer, and making use of the integral properties of §5 in the corresponding solution for \bar{A} , leads to the two key results

$$d_{21} = 0, \quad d_{22} = (2 \ln(\bar{U}') - k_2)/8, \tag{7.15}$$

where k_2 is as defined in §5.

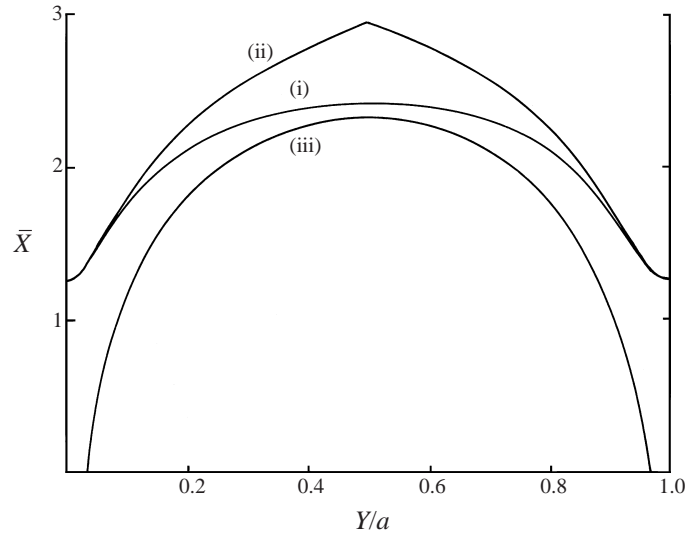


FIGURE 10. The steady-state grain boundary for the case $a = 0.6$ and $\delta = 900$ as determined from (i) the numerical solution by the contour $A = \delta^{1/2}/\sqrt{2}$, and from the asymptotic theory by (ii) the corner region solution (figure 9) and (iii) formula (6.12).

Matching (7.8) with the solution $\bar{A} = g(Y) \sinh \bar{X}$ near the wall $\bar{X} = 0$ gives

$$g = 4\sqrt{2}e^{-\bar{U}}/3 = (d_{21}\bar{U}^2 + d_{22}\bar{U}'')e^{\bar{U}}/\sqrt{2} \quad (7.16)$$

and it follows that \bar{U} is determined by the equation

$$\bar{U}''(2 \ln(\bar{U}') - k_2) = 64e^{-2\bar{U}}/3. \quad (7.17)$$

This is just the result (6.5) with δ replaced by 1 and U by \bar{U} . The required solution giving the asymptotic form of \bar{U} is

$$\bar{U} = \ln \bar{Y} - \frac{1}{2} \ln(\ln \bar{Y}) + \ln(8/\sqrt{6}) + o(1), \quad \bar{Y} \rightarrow \infty. \quad (7.18)$$

Note that for this solution \bar{U}^2 and \bar{U}'' are both of order \bar{Y}^{-2} as $\bar{Y} \rightarrow \infty$, confirming the consistency of the various expansions used in the analysis. The subtle form of \bar{U} makes it much more straightforward to construct the asymptotic solution as $\bar{Y} \rightarrow \infty$ in terms of \bar{U}' and \bar{U}'' than to use \bar{Y} directly, which would lead to complicated logarithmic expansions. The asymptote $\bar{X} \sim \bar{U}(\bar{Y})$ determined by (7.18) is shown in figure 9 and compares well with the numerical solution of the corner region problem. It also matches correctly with the main outer structure and in particular when \bar{Y} is replaced by $\delta^{1/2}Y$ is consistent with the limiting form of (6.6) as $Y \rightarrow 0$. Thus the corner region merges smoothly with the main structure in the region $0 < Y < a$ identified in §§ 4–6.

It is now possible to make a comparison between the shape of the grain boundary predicted by the numerical results of § 3 and the theoretical predictions obtained in this section and in § 6. Figure 10 shows the steady-state contour $A = \delta^{1/2}/\sqrt{2}$ obtained from the numerical solution with $a = 0.6$ and $\delta = 900$, along with the corresponding curves obtained from the corner region solution (figure 9) and the main solution (6.12). These are seen to provide reasonable approximations in their respective regions of validity, although it is clear that for the chosen values of a and

δ , the levels of approximation calculated here are insufficient to provide a clear region of overlap and thus an approximation uniformly valid for $0 \leq Y \leq a$. A quantitative estimate of the effect can be obtained by rewriting the corner region asymptote (7.18) in terms of Y . This indicates the existence of a term $-\frac{1}{2} \ln(1 + 2 \ln Y / \ln \delta)$ which must match (in part) with the term involving P_1 in (6.9). For $\delta = 900$ and $a = 0.6$ its value when $Y/a = 0.2$ is 0.49, and this explains the difference between the two approximations at that value of Y/a in figure 10. No doubt a calculation of P_1 would provide an improved estimate of the position of the grain boundary, but that is not undertaken here.

8. Core region

The main core region (region I in figure 5) is relatively unaffected by the boundary-layer structure identified above and to a first approximation simply consists of x -rolls. However, there is a very weak effect arising from the curvature of the boundary layer structure which generates a Y -dependence in the amplitude of the x -rolls in the core. This can be identified from the form of the outer boundary-layer solution (region II) as $s \rightarrow \infty$, where the solution (4.6) implies that for $\delta^{-1/2} \ll X \ll 1$,

$$A \sim \delta^{1/2} (1 - 2 \exp \{ -\sqrt{2}(\delta^{1/2} X + c - U(Y)) \}). \quad (8.1)$$

In the core $B = 0$ and it follows from (2.7) that the solution which is symmetric about $X = \frac{1}{2}$ has the form

$$A = \delta^{1/2} + R(Y) \cosh \{ (2\delta)^{1/2} (X - \frac{1}{2}) \} + \dots, \quad \delta \rightarrow \infty. \quad (8.2)$$

The function $R(Y)$ is determined by matching with (8.1) as

$$R(Y) = -4e^{-\sqrt{2}(c-U(Y))} \delta^{1/2} e^{-(\delta/2)^{1/2}} \quad (8.3)$$

and so is exponentially small as $\delta \rightarrow \infty$. Substitution for c and for $U(Y)$ using (6.6) and (6.11) gives finally

$$R(Y) = -4 \frac{(\sqrt{2}-1)}{(\sqrt{2}+1)} \frac{\delta^{(1+\sqrt{2})/2}}{(\ln \delta)^{1/\sqrt{2}}} e^{-(\delta/2)^{1/2}} \left(\frac{8a}{\sqrt{3}\pi} \sin(\pi Y/a) \right)^{\sqrt{2}}. \quad (8.4)$$

It is seen that the effect of the boundary-layer structure near the shorter sides is to generate a very weak reduction in the amplitude of the main x -roll pattern in the core relative to the finite-amplitude value that would occur in an infinite layer. This reduction is a minimum as a function of X on the centreline $X = \frac{1}{2}$ and is a maximum as a function of Y on the centreline $Y = a/2$, reducing to zero at the sides $Y = 0$ and $Y = a$. The central point of the rectangle is thus a weak saddle point of the roll amplitude. A similar amplitude deficit was identified beyond the secondary bifurcation point in the analysis and numerical computations of Daniels & Weinstein (1996, figure 5). The present result is in line with their computations which show the deficit falling rapidly in the range $70 \leq \delta \leq 200$, consistent with an exponentially small value as $\delta \rightarrow \infty$.

9. Discussion

In the present paper a novel boundary-layer structure has been identified describing the flow in regions near the side of a rectangular planform container uniformly heated from below. The boundary layer contains a mixture of rolls perpendicular and

parallel to the wall, with the perpendicular rolls dominant near the wall but their amplitude falling to zero along a transition line or grain boundary which follows a curved path between the two adjacent corners of the rectangle. The grain boundary provides a stable mechanism by which a finite-amplitude roll motion can be sustained throughout the container. It bends on a length scale x of order $\epsilon^{-1/2}$ but it, and the main boundary-layer structure surrounding it, are located at a slightly larger distance from the wall of order $\epsilon^{-1/2} \ln(\epsilon L^2)$, where $x \sim L$ is a typical measure of the horizontal dimension of the rectangle. This suggests that for finite values of ϵ , equivalent to Rayleigh numbers beyond the weakly nonlinear regime, the main boundary-layer structure has width $x \sim 1$ but is situated at a distance x from the wall proportional to $\ln L$. Whether the present structure is in fact preserved to finite values of ϵ remains to be seen. Apart from questions of stability, the width x of the transition layer of §6 is of order $L^{-2/3} \epsilon^{-5/6}$ and as ϵ increases it is possible that the fourth-order spatial derivatives will significantly influence the local form of the amplitude equations, as they do in the boundary layers of thickness $\epsilon^{-1/4}$ surrounding the whole rectangle. In principle, however, there is the prospect of using this boundary-layer approach to obtain solutions of the Swift–Hohenberg equation (2.1) for large-planform rectangular containers when ϵ is of order one; the periodic solutions in the core region are readily calculated (see for example Kramer & Hohenberg 1984; Hernandez–Garcia *et al.* 1992) and the present work provides a basis for understanding the boundary-layer structures relevant near the walls. The Swift–Hohenberg equation is of limited applicability for finite values of ϵ but the aim is to eventually use similar techniques to analyse grain boundaries and other pattern defects in the Rayleigh–Bénard system.

Sidewall structures of the type described here have been observed in Rayleigh–Bénard experiments by Croquette & Schosseler (1982) and Pocheau & Croquette (1984) for Prandtl numbers of 130 and 70 respectively. A quantitative comparison with the present theory is not possible until the theory has been extended to the Rayleigh–Bénard system for general Prandtl numbers but the qualitative features of the flow patterns, which remained stable for Rayleigh numbers of up to five times the critical value, are encouraging. In particular, most of the experimental visualizations indicate an outward curvature of the grain boundary which increases as the corners are approached, consistent with the present theory. In other experimental work for large-planform rectangular containers by Gollub, McCarriar & Steinman (1982), the visualization of the flow excluded the regions near the shorter sides of the rectangular planform. However, the slow time evolutions of the roll patterns exhibit many of the features observed by Greenside & Coughran (1984) in their numerical simulations of the Swift–Hohenberg equation, and the latter results provide strong evidence to support the existence of a stationary state of the type studied here. The numerical simulations were carried out for parameter values $a = 0.668$ and $L = 29.2\pi$ and results for symmetric initial configurations with $\epsilon = 0.03$ and $\epsilon = 0.1$ led to symmetric steady states very similar to those displayed here in figures 2 and 4. However, random initial configurations led to asymmetric final states and there is evidence to suggest that in general an asymmetric state in which the main roll pattern is curved is preferred to a straight roll pattern (Zaleski, Pomeau & Pumir 1984; see also Cross & Hohenberg 1993, p. 983). Further work is needed to investigate the existence of such asymmetric steady states and the corresponding modifications to the grain boundary structure described here. Even within the restricted class of orthogonal roll solutions studied here, for which A and B are real, there exists an ever-increasing multiplicity of steady-state solutions as δ increases. However, numerical evidence

based on using a range of different initial states in (3.5) suggests that these higher modes are unstable.

Comparison with the mechanism for wavelength selection in the corresponding one-dimensional Swift–Hohenberg equation (Cross *et al.* 1980) suggests that it is unlikely that the wavelength of the main roll pattern can take values other than the critical value associated with the onset of convection until ϵ exceeds the range L^{-2} considered here. This is because the range of possible wavelengths is limited by the size of the amplitude of convection near the boundary. Even for $\epsilon \gg L^{-2}$ the influence of the boundary-layer structure identified here may well be to inhibit the selection of new wavelengths in the main x -roll pattern, in view of the exponentially small form of the amplitude A approaching the wall. This is supported by the experimental measurements of Pocheau & Croquette (1984) which suggest that a unique wavenumber is selected for Rayleigh numbers up to five times the critical value. Similar restrictions may also apply to the wavelength of the y -roll pattern near the wall, since as $Y \rightarrow 0$ and $Y \rightarrow a$ the amplitude of this also falls to exponentially small values within the transition layer. Wavelength effects for straight grain boundaries in an infinite fluid have been studied by Manneville & Pomeau (1983), Tesauro & Cross (1987) and Malomed *et al.* (1990) but the combined influence of curvature and sidewall effects needs further consideration.

It would also be of interest to incorporate the effect of imperfect thermal conditions at the sidewalls. These tend to promote the appearance of rolls parallel to boundaries and are unavoidable in most experiments. The manner in which an imperfection determines the location of the straight grain boundary along an infinitely long isolated wall was described by Daniels & Weinstein (1992) and it would be useful, in terms of comparison with experiment, to understand how formula (6.6) for the position and shape of the grain boundary would be modified by the presence of a small imperfection. Other possible applications of the theory are to the grain boundaries observed near the perimeter of shallow circular cylinders (Croquette, Mory & Schosseler 1983; Croquette 1989*b*) where curvature is introduced naturally by the geometry of the container, and also to shallow containers of more general planform where the sidewalls are curved.

REFERENCES

- ABRAMOWITZ, M. & STEGUN, I. A. 1965 *Handbook of Mathematical Functions*. Dover.
- ARTER, W. & NEWELL, A. C. 1988 *Phys. Fluids* **31**, 2474.
- BROWN, S. N. & STEWARTSON, K. 1977 *Stud. Appl. Maths* **57**, 187.
- CHEN, M. M. & WHITEHEAD, J. A. 1968 *J. Fluid Mech.* **31**, 1.
- CROQUETTE, V. 1989*a* *Contemp. Phys.* **30**, 113.
- CROQUETTE, V. 1989*b* *Contemp. Phys.* **30**, 153.
- CROQUETTE, V., MORY, M. & SCHOSSELER, F. 1983 *J. Phys. Paris* **44**, 293.
- CROQUETTE, V. & SCHOSSELER, F. 1982 *J. Phys. Paris* **43**, 1183.
- CROSS, M. C., DANIELS, P. G., HOHENBERG, P. C. & SIGGIA, E. D. 1980 *Phys. Rev. Lett.* **45**, 898.
- CROSS, M. C. & HOHENBERG, P. C. 1993 *Rev. Mod. Phys.* **65**, 851.
- CROSS, M. C. & NEWELL, A. C. 1984 *Physica D* **10**, 299.
- DANIELS, P. G. 1978 *Mathematika* **25**, 216.
- DANIELS, P. G. & WEINSTEIN, M. 1992 *Q. J. Mech. Appl. Maths* **45**, 315.
- DANIELS, P. G. & WEINSTEIN, M. 1996 *J. Fluid Mech.* **317**, 111.
- FRIEDEL, J. 1964 *Dislocations*. Addison-Wesley.
- GOLLUB, J. P., MCCARRIAR, A. R. & STEINMAN, J. F. 1982 *J. Fluid Mech.* **125**, 259.
- GREENSIDE, H. S. & COUGHRAN, W. M. 1984 *Phys. Rev. A* **30**, 398.

- HARI, A. & NEPOMNYASHCHY, A. A. 1994 *Phys. Rev. E* **50**, 1661.
- HECKE, M. VAN & MALOMED, B. A. 1997 *Physica D* **101**, 131.
- HERNANDEZ-GARCIA, E., SAN MIGUEL, M., TORAL, R. & VINALS, J. 1992 *Physica D* **61**, 159.
- HOYLE, R. B. 1995 *Phys. Rev. E* **51**, 310.
- KRAMER, L. & HOHENBERG, P. C. 1984 *Physica D* **13**, 357.
- MALOMED, B. A. 1994a *Phys. Rev. E* **50**, 3310.
- MALOMED, B. A. 1994b *Phys. Rev. E* **50**, 1565.
- MALOMED, B. A., NEPOMNYASHCHY, A. A. & TRIBELSKY, M. I. 1990 *Phys. Rev. A* **42**, 7244.
- MANNEVILLE, P. & POMEAU, Y. 1983 *Phil. Mag. A* **48**, 607.
- MILES, J. W. 1978 *Proc. R. Soc. Lond. A* **361**, 277.
- NEWELL, A. C., PASSOT, T. & SOULI, M. 1990 *J. Fluid Mech.* **220**, 187.
- POCHEAU, A. & CROQUETTE, V. 1984 *J. Phys. Paris* **45**, 35.
- POMEAU, Y. & ZALESKI, S. 1981 *J. Phys. Paris* **42**, 515.
- ROSALES, R. R. 1978 *Proc. R. Soc. Lond. A* **361**, 265.
- RUBINSTEIN, J., STERNBERG, P. & KELLER, J. B. 1989 *SIAM J. Appl. Maths* **49**, 116.
- SCHLUTER, A., LORTZ, D. & BUSSE, F. H. 1965 *J. Fluid Mech.* **23**, 129.
- SIVAPRAGASAM, V. R. 1995 Finite amplitude patterns of convection near a lateral boundary. PhD thesis, City University, London.
- SWIFT, J. B. & HOHENBERG, P. C. 1977 *Phys. Rev. A* **15**, 319.
- TESAURO, G. & CROSS, M. C. 1987 *Phil. Mag. A* **56**, 703.
- ZALESKI, S., POMEAU, Y. & PUMIR, A. 1984 *Phys. Rev. A* **29**, 366.